Survey on New Strategies and State of the Art for Space Debris Catalogue Generation for Optical Sensor Networks

Guido Pedone
Airbus Defence and Space GmbH
Jens Utzmann
Airbus Defence and Space GmbH

Roger Förstner
Universität der Bundeswehr München

ABSTRACT

The rise of new satellite constellations, especially in the LEO region, together with an increasing number of new launches and wider participation in space-related activities from various entities is pushing Earth orbits toward maximum capacity. Together with the necessity of a worldwide set of regulations for the Space Traffic Management (STM), there is the need to provide a proper surveillance support for the cataloguing of the increasing number of uncooperative space objects, e.g. launchers bodies, dismissed satellites and fragmentation events.
Differently from radar facilities, in-space and on-ground optical observers can offer additional data and cover higher orbital regions with reduced energy consumptions. Optical sensors offer the possibility to deal with illuminance information of the objects, the albedo information and the change of measured magnitude over time. This information can be combined to perform initial object characterisation (e.g. shape and attitude information). However, a certain number of constraints come together with optical sensors: mechanical-constrained slewing capabilities, narrow fields of views, illumination constraints such as the objects need to be in direct Sunlight and local darkness (night) in case of ground station observer.
This paper opens with a state of the art review of the common data processing techniques and observation strategies for Catalogue Generation, followed by the description of a new method for the re-observation of short arcs. The state of the art summarizes the requirements coming from the correlation and initial orbit determination cataloguing tools necessary for the creation of a catalogue of space objects. The new method will consider post-processing strategies to keep track of new detections using Constrained Admissible Regions (CAR) to triangulate possible objects that may have generated the measurements. A proper triangulation of the CAR generated by a short arc, together with some refinement filtering techniques in case of more measurements, will allow the generation of a family of Virtual Debris (VD). Eventually, a proper covariance matrix can be associated to each family of VD and their future observability studied. The work and the simulation presented during this paper take place in the framework of the Airbus Defence and Space SSA department, where this research has been conducted. The software tool SPOOK (Special Perturbations Orbit determination and Orbit analysis toolKit) used during the simulation has been presented already in [6], [12] and [2] together with the sensing facilities, such as the Airbus Robotic Telescope (ART) in Spain, used for real observation campaigns.
The observation strategy will be presented as completion of a wider cataloguing system that can be fed by different sources, i.e. Space-track online catalogue and SMARTnet participation. However, special attention will be given to the Catalogue Generation chain that is the first essential part of a cataloguing system.

1. INTRODUCTION

The main product for Space Surveillance and Tracking is to build-up and maintain a catalogue of Resident Space Objects (RSO). The information contained inside a catalogue, when updated and trustable (i.e. object state vector known within a certain uncertainty envelope), can be used as support for the main monitoring and mitigation of space debris activities, as: collision warning, event monitoring and active debris removal (ADR).

Current catalogues, such as the publicly available space-track.org, maintain inside their databases about 28600 RSO [4]. Eventually these numbers are going to increase, as new radar and sensor network facilities became operative[1], even by one order of magnitude. This will open new challenges for the operative maintenance and processing operations of catalogues.
Radar sensor facilities find a suitable operation field on low orbits (LEO) objects scanning where they can rely on large scanning volumes with a sustainable beam power intensity. Optical resources, on the other hand, do not require signal emission and the lower power consumptions make them very suitable for higher orbits detections. However, both for Radar and Optical observers, the challenge to pass from new detections to an orbit identification is tricky. Since the high velocity of LEO objects, Radar back-scattering may produce few measurements per passage. On the other hand, narrow Field Of View (FOV) of telescope may lead to similar results for higher orbit objects.
Short passages of objects, from now on referred to as short arcs, may not contain enough information for a preliminary orbit reduction and the object that generated them may be lost or bad-linked. This paper aims to give a high level overview of the operative techniques and state-of-the-art research on that specific aspect of a Catalogue Generation. The standard flow chart of a Catalogue Generation loop can be seen in Fig. 1. In this flow chart, a new block has been added, connected with dashed lines, that considers the observation planning part: the closing ring of the chain.

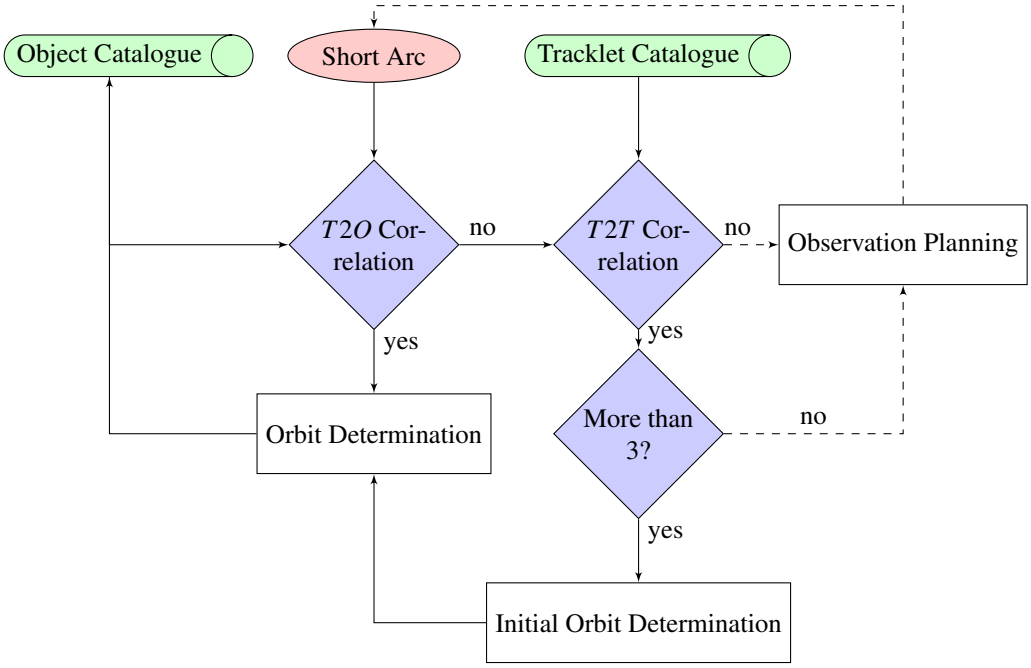

Fig. 1: Standard Catalogue Generation flow chart, plus observation planning block as closing ring of the chain. Inside the two above decision blocks: $T2O$ stands for Tracklet-to-Object and $T2T$ for Tracklet-to-Tracklet.

The standard flow of operations consists of the following steps:

1. A short arc is detected by a sensor;
2. The short arc is tried to be correlated to a known object inside a catalogue, in a process called tracklet-to-object correlation;
   (a) If an object can be associated to that tracklet, Orbit Determination (OD) is performed;
3. if the catalogue correlation is unsuccessful, the short arc is tried to be correlated with another uncorrelated tracklet;

[1] See the Space Fence on Kwajalein Atoll [1].

4. if the tracklet-to-tracklet correlation is successful and more than 3 tracklets can be correlated to each other, an Initial Orbit Determination (IOD) is performed followed by a full orbit determination of the new object state vector.

It is worth highlighting that every time a new Initial Orbit is triggered, a new object instance is added to the Object Catalogue. From that, it is clear that the first goal of Catalogue Generation is to observe passages of unknown objects whose observed tracklets cannot be directly correlated to already-known objects.
This paper will focus on the closing ring of this chain: the observation planning part. When no information from the object we are going to observe can be known a-priori, observation planning must make use of some other sources of information - e.g. the orbital class of the objects targeted by the survey campaign and preliminary information that can be extracted from the short arc. In order to clarify these two aspects, an introduction on operative state of the art (SoA) will be given in the next section 2. After that, one Catalogue Generation technique will be presented together with some simulation results in section 3. Finally, in section 4 the conclusion will be given.

2. SOA AND OBSERVATION REQUIREMENTS

The following section will describe the high level requirements, based on current and operative state-of-the-art studies and technologies, to perform surveys for Near Erath Objects (NEO) detection.

2.1 Observation Properties

Depending on the type of sensor available, different observation properties must be considered. However, for this paper more level of detail will be given to optical telescopes.
An optical observation of a space debris from a ground station, has usually the following constraints:

- the object must be illuminated by the Sun. Moreover, the phase angle (geometrical angle between the source of light, the object and the observer) should be as small as possible;
- the object should not be inside the cone of the Earth shadow;
- the object should not overlap other bright sources of light - e.g. the Moon, the Milky Way, bright stars...
- the observation should be performed in dark conditions, i.e. the Sun below the horizon;
- the target should be within the Fiel of Regard (FoR) of an observer (e.g. respecting minimal and maximum elevation).

From a space observer, just the first three constraints of the previous list are still applicable. Additionally, the Earth limb constraint (usually between 100 and 150 km) should be taken into consideration.
Optical observations are performed without the need of a signal emission by the sensor, but are collecting the light that from another source (i.e. the Sun) that is scattered by object in space. The driving quantity for optical observation is the Signal-to-Noise S/N ratio. In order to detect a feature crossing the Field-of-View (FOV) of a telescope, the observation must be performed when the average background light level is low (e.f. during the night).
A full astronomical reduction of the images usually requires an higher observation quality (Nautical Sun-set with the Sun below -9 deg the horizon), and a certain number of stars visible within the image FOV. Less severe requirements can relax the previous constraints, and recent literature [14] suggests that also daylight images for bright LEO objects can be photometrically reduced.
As support for the next sections, it is useful to introduce the concept of observable. The output of a space object observation is constituted by the coordinates of the object in the sky. The observable is defined as the set of those coordinates that can be directly retrieved from an observation. In the case of optical observations, the observable is constituted by the angular coordinates: right ascension α, declination δ and their respective relative rates $\dot{\alpha}$ and $\dot{\delta}$. For radar observation usually the observable contains the range, the azimuth and elevation position of the object (Additionally Doppler radars can provide also the range rate information).

2.2 Image Processing

The highest contribution to the accuracy of optical observations is defined by the quality of the image processing chain. Before entering into details, a distinction needs to be done between astrometric and photometric reduction of images. Astrometric reduction contributes to the highest astrometric precision for the coordinates of features in the images. Calibration results [2] show that even sub-pixels precision level can be reached in this framework. On the other hand, with photometry reduction of an image, it is meant only the evaluation of photometric quantities (e.g. received signal, background noise) of the observed features in the image. One of the key quantity to assess the detectability of a feature is the S/N ratio, as introduced in 2.1. The S/N is a function of the absolute magnitude of the light source, the distance and the relative angular velocity between the light source and the observer and the noise. In [9] is provided a detailed definition of the S/N and its calculation. In particular, the effects of the trailing losses are analysed. In fact, observation strategies for unknown objects for Catalogue Generation usually require sidereal (or similar) pointing of the sensor FOVs, that together with high LEO objects angular velocities, may lead to long streak observations of the debris. In that case, the signal is "spread" on a wider area or *trail*.
The next step after image processing is constituted by the Tracklet Linking. As presented in [12] and [2], the tracklet linking is the linkage of the measurements obtained by the image processing to identify possible NEO and remove false measurements and stars. Main sources of error on this steps, especially for LEO streak observations, are the relative low precision of streak central pixels (factor dependent on the power of signal received, see [9]), the general unpredictability of streak lengths for features close to the image border and the usually low number of measurements available. New multi-target tracking techniques, as presented by Früh in [7], may allow different multi-hypothesis strategies to deal with a real-time single measurement association. In this way tracklet linking, correlation and object information improvement (processes that will be described in the next sections) can be combined in a single processing block.

2.3 Tracklets Correlation

Tracklet correlation can be identified as a preliminary step before Orbit Determination (OD). Sometimes it can be referred to as linkage [10]. The aim, in fact, is to link an observed tracklet with the object that may have originated it or to another unknown tracklet.
Starting from Milani [10] Virtual Debris (VD) hypotesis linkage to Multi-Hypotheses and Gaussian Mixture Models [5], [3], Admissible Regions constitute a suitable technique for hypothesis generation starting from single tracklet observations.

2.3.1 Admissible Region

The concept of admissible region, has been introduced by Milani [11] and Tommei [16]. Recalling the previously defined definition of observable, and the ways in which it is possible to uniquely identify an object in space $\boldsymbol{x}$ (6 quantities at least + time), it is common to have a subset of elements $\boldsymbol{A}$ in a state vector that are directly retrievable from the observable and a subset of elements $\boldsymbol{B}$ that are not, $\boldsymbol{x} = [\boldsymbol{A}, \boldsymbol{B}]$. If no more measurements can be provided and orbit determination techniques cannot be triggered, the subset of elements not directly retrievable from the observable are usually undefined and may assume every possible value. The idea behind the Admissible region is to constrain the regions of possible solutions for this undefined sub-set of options. A precise presentation of the Admissible Regions and Constrained Admissible Regions is out of the scope of this paper, however it is worth mentioning the case of a typical optical observation. A possible way to define the state vector of a NEO object can be using the following notation:

$$\boldsymbol{x} = \left[\alpha, \delta, \rho, \dot{\alpha}, \dot{\delta}, \dot{\rho}\right] \tag{1}$$

where α is the right ascension of the objects, δ the declination and ρ the range, or distance to the observer. This notation is especially suitable for optical observation where the subset of directly retrievable quantity from the observable is straightforward, being the optical observable equal to $\boldsymbol{A} = \left[\alpha, \delta, \dot{\alpha}, \dot{\delta}\right]$, that is also called attributable. The attributable is usually obtained with a Weighted Least Squares (WLS) linear regression technique starting from the set of observables contained in a short arc tracklet. An example of Constrained Admissible Region (CAR) for an optical observation is shown in Fig. 3. As shown, the CAR is the region of the range/range-rate plane where to look for possible solutions of the real state vector of the object.

2.3.2 Virtual Debris

The concept of Virtual Debris or VD comes from a proper sampling of the CAR to obtain feasible orbital solutions. The sampling of a CAR can be performed via equispaced grids in the range and range-rate axes or iso-energy lines [5] inside the graph. A fast and good solution to this is given by [11] [10] using the Delaunay Triangulations and this technique will be also used for the implementation of the VD algorithm shown in the simulation section.
The sampling of the CAR is so performed:

- first, equispaced boundary n points are calculated;
- second, a first Delaunay triangulation is performed on those points and $N_{triangles}$ ($\leq 2 \cdot n + 1$) triangles are generated;
- third, an iterative loop creates new points and new triangles (keeping the Delaunay properties valid) inside each barycenter of the current triangles. Some rules are here respected like uniform density of the points, minimum area of the triangles and maximum number of samples.

For each vertex of those triangles a VD is associated, that corresponds to a possible solution of the orbit. A virtual debris will have so the shape:

$$\boldsymbol{X}^i = \left[\boldsymbol{A}, \boldsymbol{B}^i\right] \; i = 1, N_{vertex} \tag{2}$$

Where N_{vertex} corresponds to the number of vertices of the triangles constituting the Delaunay triangulation. To each VD can be later associated a normal $\boldsymbol{C}$ and covariance matrix $\boldsymbol{\Gamma}$ [10], based on sensor accuracy and the WLS variance results obtained when evaluating the attributable $\boldsymbol{A}$ and the streak length. Additionally, each VD has associated an observation matrix $\boldsymbol{H}$ and a precise epoch or instant of time t^i. The last will be generally slightly different for each VD due to the light-time corrections that shall be applied for each set of range.
The normal matrix $\boldsymbol{C}_A$ corresponds to the pseudo-inverse of the covariance matrix:

$$\boldsymbol{\Gamma} = \begin{bmatrix} \boldsymbol{\Gamma}_A & \boldsymbol{0} \\ \boldsymbol{0} & \boldsymbol{0} \end{bmatrix} \tag{3}$$

Where $\boldsymbol{\Gamma}_A$ is directly retrievable from the first measurements of the tracklet used for the attributable initialization. Such a set of VD, can be so propagated for future time steps together with its covariance. When new measurements become available, a new attributable $\boldsymbol{A}_2, \boldsymbol{C}_2$ can be calculated, and an attribution penalty can be evaluated for each VD [10]:

$$K_4^i = \left(\boldsymbol{A}_2 - \boldsymbol{A}^i\right) \cdot \left[\boldsymbol{C}_2 - \boldsymbol{C}_2 \boldsymbol{\Gamma}_0 \boldsymbol{C}_2\right] \left(\boldsymbol{A}_2 - \boldsymbol{A}^i\right), \;\; \boldsymbol{\Gamma}_0 = \left[\boldsymbol{C}_2 + \boldsymbol{C}_{A^i}\right] \tag{4}$$

Case-by-case (mainly depending on the observed orbital region) a value of K_{max} can be found for which filter out all the VD with a $K_4^i > K_{max}$.

2.4 Orbital Information Improvements

The cataloguing pipeline implemented in Airbus DS has been presented in [12] and [2]. Once the tracklets have been correlated to a known object, the measurements can be used to update the orbital information on that object and reduce the covariance of its state vector. In the case the tracklet does not allow any linkage with an object in a catalogue, more tracklets can be associated to each other to produce an Initial Orbit Determination. Common IOD techniques involve the Gauss's method and are usually followed by a Weighted Least Square reduction of the guessed orbit with all the available measurements. However, techniques involving the sampling of the admissible region like the Gaussian Mixture Model definition [3] may produce directly an orbit guess after the tracklet correlation [9].

2.5 Survey Observation Strategies

Observation strategies for Catalogue Generation have generally in common the idea that the objects of observation (the NEO spacecraft and debris) are, a-priori, unknown. Despite the huge progress and wide literature offered in all the aspects of the catalogue generation tasks (from image processing to orbit determination), the definition of an optimal strategy to cover the whole NEO population in the most efficient way is difficult to be formulated.
Some special cases may allow the formulation of dedicated observation strategies, for example:

- **Real-Time Tracking:** fast image processing tools, avoiding astrometric reductions, or involving fast masking techniques for pattern matching in a series of images [15], may allow a real-time tracking scenario for unknown NEO. Such a technique, typically referred to as *stare-and-chase* scenario, uses a first sidereal pointing to a fixed position in the sky and triggers some closed-loop control tracking device as soon an object appears inside the FOV. Operative examples of this have been presented for Laser imaging in [13].
- **Sidereal Monitoring:** Optimization methods may be applied to evaluate the best observation pattern for sky mapping, starting from big catalogues or population models of objects in which the Catalogue Generation can be interested. Such patterns can be very different depending on the objects of interest, and are very suitable for crowded regions like the GEO belt or the low elevation area close to the border of the Earth shadow during Sun set or Sun rise where most of the LEO objects are visible.
- **GEO Blind Tracking:** A special case of the previous point can be done for the GEO belt, the region in space around 0° declination where most of the GEO satellite are present. In this special case, the sidereal survey can be substituted with a Earth-fixed survey (the observer does not move) and the GEO objects with low inclination values will appear as point features in the images. Examples of such observation techniques have been presented as implemented in SPOOK in [12] and [2].

3. SIMULATION OF NEW SURVEY STRATEGY

Following the results described in [11] and [3], it appears that the usage of Admissible Regions can be a suitable direction for Catalogue Generation strategies. When short arc observations cannot cover enough orbit for a proper state vector identification, it is necessary to adopt some other techniques other than the classical Gauss's orbit determination to not lose the information that few measurement instances may contain.
The idea is to identify a survey strategy that is able to keep track and follow all the possible cloud of orbital solutions that may have generated the short arc observation, with a strategy similar to Catalogue Maintenance (CM). In this case, the *catalogue* to maintain is composed by the set of Virtual Debris directly obtainable from a short observation. With respect to typical optical sensor tracking tasks, this observation strategy is most common to be applied to LEO target. In fact, LEO objects may generate more easily and with a higher frequency of short passages in a sidereal survey scenario. These operation conditions are affected by the following issues:

1. very fast objects are usually outside the slewing operability of ground telescopes facilities;
2. LEO objects from the same constellation or result of a fragmentation event can be close enough in the observer FOV to not allow a proper correlation of the obtained tracklets.

For reason number 1, the observations shall be conducted in a sidereal survey frame. Keeping the telescope on an inertial pointing. That means, to compensate only the Earth angular rotation. For reason number 2, instead, the observations shall be scheduled in a time span of several days and, if possible, more passages per day. The last point is necessary to have a proper coverage of the orbit of the single objects and allow a correct correlation and eventually orbit determination.

3.1 Virtual Debris Algorithm

In Fig. 2, it is schematized an example of Virtual Debris algorithm implemented during this simulation.
The starting point of the survey scenario is a set of observed short passages. For each observed tracklet only the first 2 measurements are considered at the beginning to extract a possible CAR. Out of the CAR, using a proper Delaunay's triangulation, an optimal sampling of VD is performed. If there are more than 2 measurements in the tracklet resulting from the object's short passage, the VD are filtered based on the Attribution Penalty information. Additionally, a proximity filter is executed to remove VD that are too close to each other. The last step is necessary since the tracklets may be very close to each other and the generated VD clouds could be superimposed.
Out of the iterative loop, when all tracklets have been processed, the VD list is propagated in time and measurements are used to schedule observation tasks for each observer. To understand the meaning behind the CAR and the attribution penalty filtering, the example presented in Fig. 3 can be considered. In this case, it has been considered a GPS object (NAVSTAR 73, norad 40534) observed by ART on the night of 9^{th} of March 2021. The CAR has been obtained constraining: the semi-major and minor axes to be between 20000 and 30000 km and the eccentricity below 0.5. On

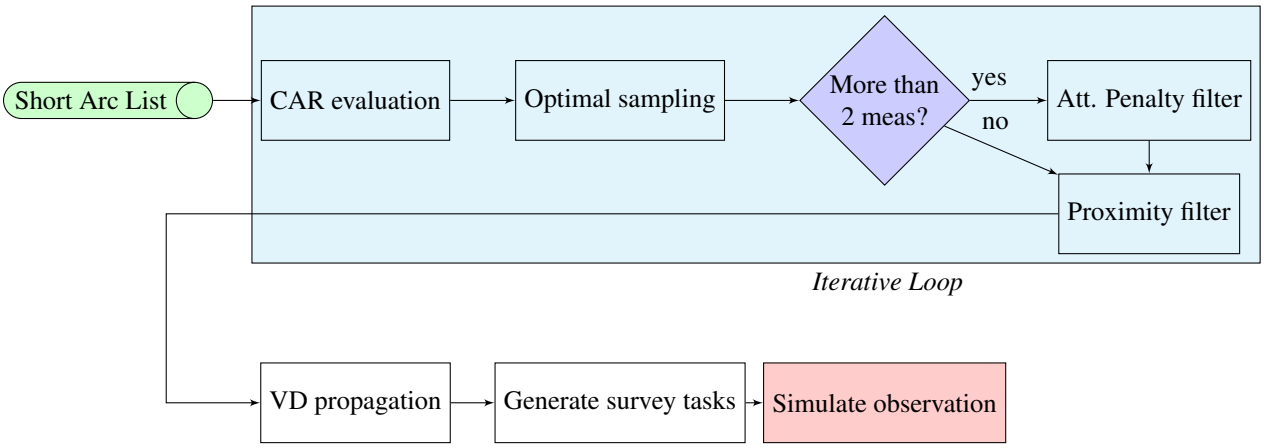

Fig. 2: Catalogue Generation after short arc measurement flow chart.

the top of the figure it is visible the CAR in range and range-rate graph, together with the VD samples and the real object position obtained from its ephemeris. On the bottom of Fig. 3, instead, it is visible a close-up of the same CAR to show the values of the calculated attribution penalty for each VD. As visible from this image, the attribution penalty region is able to constrain further the region of VD around the real object position. In that case, the specific factor that has been constrained applying this filter is the predicted eccentricity value of the orbit.
As said, the observations are scheduled accordingly to the predicted passages of the VD over the observer accessibility sphere. An example of an observation plan for the same GPS object as before is visible in Fig. 4. The observation plan is obtained as follows:

1. first it is evaluated the average angular velocity of the all VD set for all the night. That value is used to design the task duration of each observation field ($\Delta t_{field} = FOV_{size}/mean\ angular\ velocity$).

2. Each task of the observation plan is composed by a single field, during which, the pointing of the telescope remains fixed to the same sidereal position. The pointing direction is evaluated considering the positions of all the VD, at the specific time step during which the observation field has been designed. First, it is evaluated the direction of motion in the right ascension - declination plane to understand if the ”cloud” of VD is rising over the observer (moving upward) or setting (moving downward). If the ”cloud” of VD is moving upward, the pointing direction will be selected with the position of the highest object in declination (that will be the first to be lost). Vice versa, if the ”cloud” is setting, the lowest VD position in declination will be selected as pointing direction.

3. after each field, a settling time of 40 seconds is considered to account for the slewing and setting time of the camera of the observer.

4. if no VD are currently accessible by the observer, no observation is scheduled.

3.2 Simulation and Results

As simulation scenario, it has been selected a hypothetical catastrophic event of a collision between two LEO objects: the micro-satellite *SEDSAT 1* norad 25509 and the Starlink satellite 1730 norad 46563. The close conjunction happened on 24^{th} of June 2021 at 18:07:16. The conjunction has been predicted with the new SPOOK's conjunctions screening tool, [2] [12]. The predicted absolute relative distance at time of conjunction was 90.94 m with a relative velocity of $5.7260\,\mathrm{km\,s^{-1}}$. Accordingly to the literature [9], a collision can be considered to be catastrophic when the ratio between the kinetic velocity of the projectile and the mass of the satellite is over $40000\,\mathrm{J\,kg^{-1}}$. Threshold largely reached in this case. The fragmentation event has been simulated with the SPOOK's fragmentation tool that uses the same fragmentation model of NASA's EVOLVE 4.0 as presented in [8]. The fragmentation results are visible in the Gabbard plot in Fig.s 5, 6 and 7.

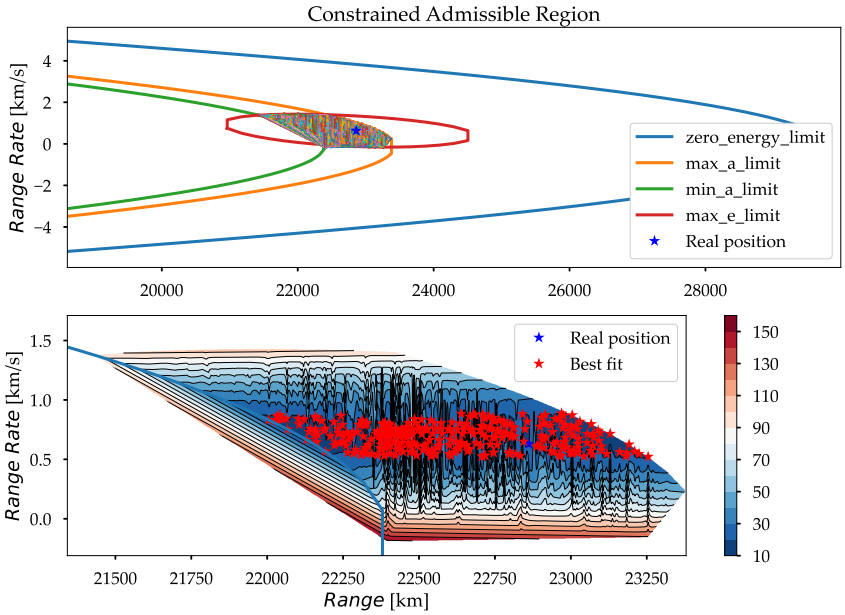

Fig. 3: Constrained admissible region obtained with a real observation of the GPS object norad 40534 on 9 of March 2021. On the top the figure, in the range and range-rate graph the CAR is visible and the constraint lines from which has been formed. On the bottom, a close-up of the same region with a colour plot for the attribution penalty value calculated for each VD. In both graphs the real position of the GPS object can be seen, obtained from its ephemeris.

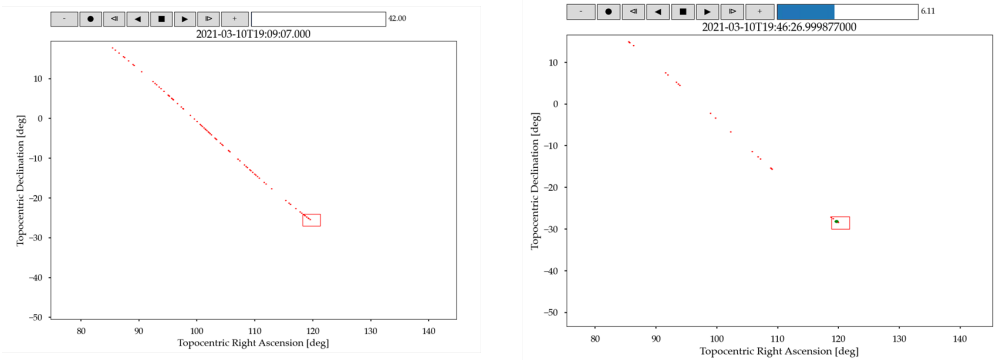

Fig. 4: Captions from the visualization tool in the observable plane (right ascension and declination) for the observation plan obtained with the VD algorithm. The red square corresponds to the observer's FOV, while the dots correspond to the VD predicted positions. Eventually, after some time in the simulation, the real object (the green dot) is observed.

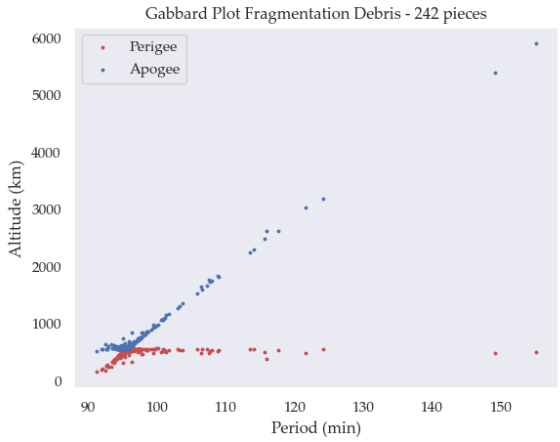

Fig. 5: Gabbard plot of the debris distribution originated after the simulated collision between object norad 46563, considered as the target, and the object norad 25509, considered as the projectile on 24^{th} of June 2021 at 18 : 07 : 16. The Gabbard plot shows the distribution of apogee and perigee radii for all the fragments of the collision.

Table 1: Characteristics of the sensors used during the simulations:

Name	Coordinates	FOV dimension	Sensor accuracy
ART	$-6.63°$W $38.22°$N	$\varnothing = 2.43\,\text{deg}, 1.38\,\text{deg}$	$\sigma_\alpha = 0.5'', \sigma_\delta = 0.5''$
CG_AUS_1	$145.786°$W $-27.481\,05°$N	$\varnothing = 3.0\,\text{deg}, 3.0\,\text{deg}$	$\sigma_\alpha = 1'', \sigma_\delta = 1''$
CG_FPO_1	$-149.4826°$W $-17.6641°$N	$\varnothing = 3.0\,\text{deg}, 3.0\,\text{deg}$	$\sigma_\alpha = 1'', \sigma_\delta = 1''$
CG_FGU_1	$-53.4916°$W $3.6685°$N	$\varnothing = 3.0\,\text{deg}, 3.0\,\text{deg}$	$\sigma_\alpha = 1'', \sigma_\delta = 1''$
CG_ARG_1	$-69.0801°$W $-35.8522°$N	$\varnothing = 3.0\,\text{deg}, 3.0\,\text{deg}$	$\sigma_\alpha = 1'', \sigma_\delta = 1''$
CG_USA_1	$-76.1975°$W $41.1947°$N	$\varnothing = 3.0\,\text{deg}, 3.0\,\text{deg}$	$\sigma_\alpha = 1'', \sigma_\delta = 1''$
CG_SCA_1	$-14.042°$W $28.310\,89°$N	$\varnothing = 3.0\,\text{deg}, 3.0\,\text{deg}$	$\sigma_\alpha = 1'', \sigma_\delta = 1''$

For this simulation, a 7-sensors[2] network has been considered, as visible in Tab. 1, where are listed their characteristics and locations. For simplicity of the simulation, the Starlink satellite has been considered to have a mass of 260 kg and a characteristic length of 5 m. The results of the fragmentation simulation totally found 262 objects greater than 10 cm. The physical properties, visible in Fig. 7, have been used as an initialization parameter for each object for the next simulation, during which the objects generated will be propagated for a time span of 10 days from the epoch of the collision. A visualization rendering of the propagation of the debris positions after the collision at two different time steps is visible in Fig.s 8 and 9. This simulation is so composed:

1. First, the collision's debris are propagated for all the simulation time.
2. During the collision, the sensors are simulated to point in the direction of the conjunction (if accessible). See, conjunctions planner of SPOOK in [12].
3. Observations are simulated for the first sensor who is able to observe the immediate new passage of the debris cloud after the collision. In that case, it was the Argentinian observer *CG_ARG_1*.
4. To be conservative, out of the whole set of 262 observable debris, only a 20% of them has been considered able to generate successfully linked tracklets. And 50 tracklets have been considered as first set of measurements to set the VD algorithm, as in Fig. 2.
5. The observations have been simulated as follows:

[2]The sensors used in this work are to be considered not real. Selected by the author accordingly to the principle of the best coverage in the 5 continents.

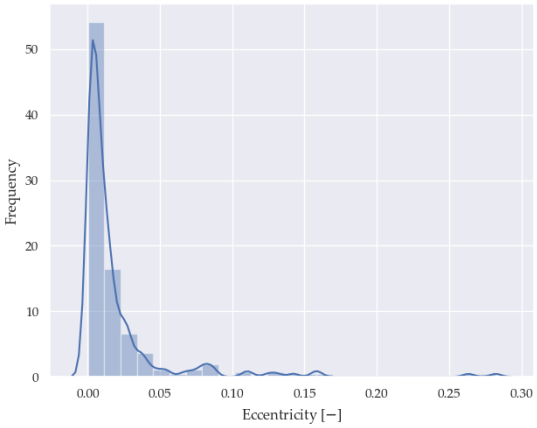

Fig. 6: Eccentricity distribution of the orbits of the fragments result of the collision.

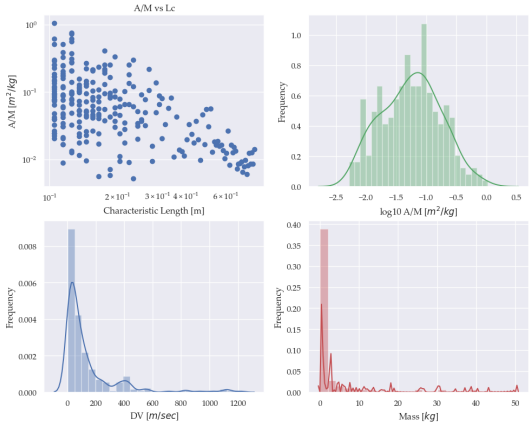

Fig. 7: Physical properties' distribution of the collision debris. On the top left: the distribution of the Area-to-Mass A/M ratio in logarithmic scale with respect to the characteristic size of the object. On the top right: the count of objects for each A/M ratio value. On the bottom left: the distribution of fragments accordingly to the Δv perturbation of the Debris from the master object (the Starlink satellite). On the bottom right: the distribution trend of the objects accordingly to their Mass.

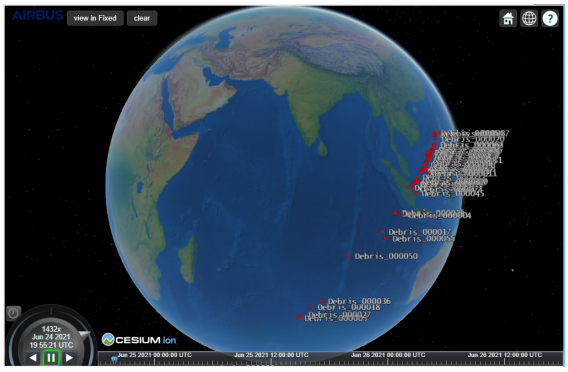

Fig. 8: Fragment debris orbit visualization 1 hour after after the collision event.

Fig. 9: Fragment debris orbit visualization 7 hours later the collision event.

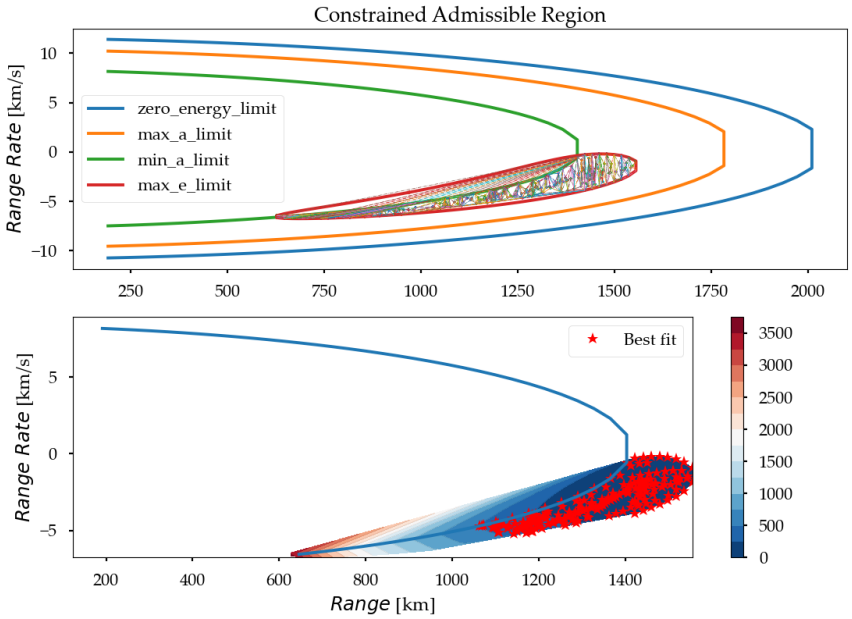

Fig. 10: LEO example of a CAR. Generated by one of the observed fragments by observer in Argentina on $24^{(th)}$ June 2021.

- Processing time of 6 hours (to be conservative);
- Observation by the full network for 1 day.

The simulation has been done for 10 consecutive days of observation, from 25-06-2021 to 07-07-2021.
All the observations have been planned to be sidereal with a 0.1 s exposure time. In this way the trailing losses are reduced to minimum and the observers do not need to perform active tracking of such fast objects.
In Fig. 10 it is shown an example of CAR region obtainable from a short arc observation of a fragment object. For all the simulations, the minimum tracklet length for a short arc to be processable has been considered to be 3 measurements. For safety reasons, the first measurement in a tracklet has always been neglected, since it is usually associated with the maximum noise level. The 2^{nd} and 3^{rd} measurements are used to compute the first CAR area, using the following constraints:

- minimum range from the observer: $0.03 \cdot R_{Earth} \approx 191.34\,\text{km}$;
- maximum range from the observer: $3 \cdot R_{Earth} \approx 19.134\,\text{km}$;
- maximum eccentricity: 0.25;
- minimum semi-major axis: 6500 km;
- maximum semi-major axis: 16 000 km.

The typical length of a tracklet is between 3 and 5 measurements.

The results of this simulation, partially shown in Fig.s 11 and 12, are a total of 230 objects (out of the 240 objects with eccentricity below 0.25 originated from the fragmentation) observed. Among them, only 178 debris have been observed more than 3 times in 3 different passages, that is the condition for a proper *Tracklet-to-Tracklet* correlation initialization (see Fig. 1).

The 90% of the observed debris, around 208 objects, have been observed at least two times. These results may increase further if the VD algorithm would be initialized with an higher number of tracklets after the fragmentation

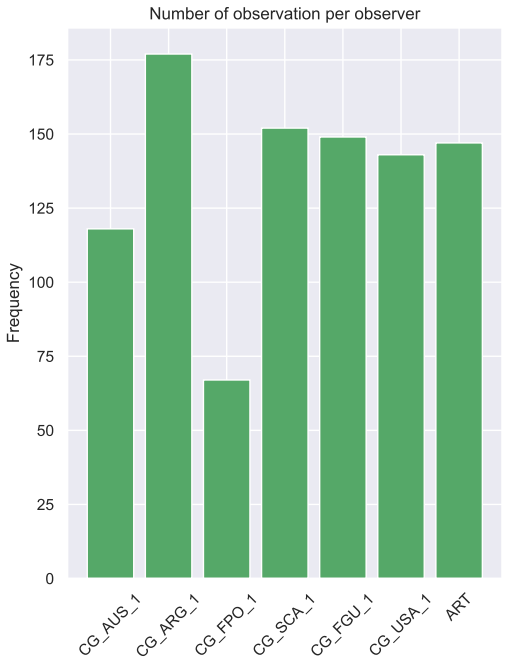

Fig. 11: Number of observations for each observer during all the simulation.

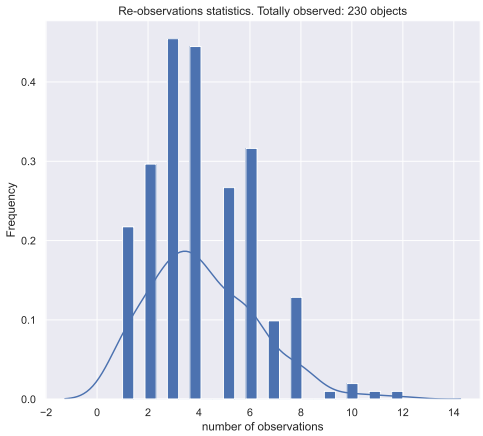

Fig. 12: Observation statistics of revisits for all the observed debris.

event, instead of the 20% of tracklets utilized in this simulation, and considering less restrictive processing times. In this simulation, the processing of short arcs for the VD algorithm has been considered to be operated with a centralized processing unit and considering a total of 6 hours of time span to process the images, collect the measurements and execute the VD algorithm pipeline.

4. CONCLUSION

The purpose of this paper is to show the main aspects and challenges connected with the observation strategy planning for Catalogue Generation. Literature is wide in the field of image and data processing, allowing simpler observation strategy definitions. Especially for LEO regions surveys, optical observations may be used to trigger Admissible Regions' construction of orbital solutions like the VD algorithm presented in this paper.
The VD algorithm presented in this paper shows its applicability to LEO objects observation and results have been shown in the case of a fragmentation debris detection. The limiting factor of optical sensing for LEO orbit survey are the high angular rates of the objects that leave short passages on a sidereal pointing FOV. To overcome that, one of the future development directions for Catalogue Generation scenario is the construction of fast real-time tracking *stare-and-chase* scenarios.

REFERENCES

[1] U. S. F. P. Affairs. *USSF announces initial operational capability and operational acceptance of Space Fence*. 2020. URL: "https://www.spaceforce.mil/News/Article/2129325/ussf-announces-initial-operational-capability-and-operational-acceptance-of-spa/" (visited on 07/08/2021).

[2] G. Cirillo, M. G. V. Dimitrova, J. Utzmann, et al. "Performance of Airbus Robotic Telescope and the SST Data Processing Framework SPOOK". In: *ESA Space Debris Conference* May (2021).

[3] K. J. DeMars and M. K. Jah. “Probabilistic initial orbit determination using Gaussian mixture models”. In: *Journal of Guidance, Control, and Dynamics* 36.5 (2013), pp. 1324–1335.

[4] ESA. *Space debris by the numbers*. 2021. URL: "https://www.esa.int/Safety_Security/Space_Debris/Space_debris_by_the_numbers" (visited on 07/08/2021).

[5] O. R. Fernandez, J Utzmann, U Hugentobler, et al. “Correlation of Optical Observations to Catalogued Objects using Multiple Hypothesis Filters”. In: January (2019), pp. 22–24.

[6] O. R. Fernandez, J. Utzmann, and U. Hugentobler. “SPOOK-A comprehensive Space Surveillance and Tracking analysis tool”. In: *Acta Astronautica* 158 (2019), pp. 178–184.

[7] C Frueh, H Fiedler, T Schildknecht, et al. “Multi-target tracking for smartnet : multi-layer probability hypothesis filter for near-earth object tracking”. In: May (2021), pp. 20–23.

[8] N. L. Johnson, P. H. Krisko, and J Liou. “Nasa ’ S New Breakup Model of Evolve 4 . 0”. In: 19.1 (1998), pp. 1377–1384.

[9] A. Milani, D. Farnocchia, L. Dimare, et al. “Innovative observing strategy and orbit determination for Low Earth Orbit space debris”. In: *Planetary and Space Science* 62.1 (2012), pp. 10–22. arXiv: 1106.0168.

[10] A. Milani and G. F. Gronchi. *Theory of Orbit Determination*. 2008, p. 382.

[11] A. Milani, G. F. Gronchi, M. D. M. Vitturi, et al. “Orbit determination with very short arcs. I admissible regions”. In: *Celestial Mechanics and Dynamical Astronomy* 90.1-2 (2004), pp. 59–87.

[12] G. Pedone, D. Vallverdu Cabrera, M. G. Dimitrova Vesselinova, et al. “Spook: A Tool for Space Objects Catalogue Creation and Maintenance Supporting Space Safety and Sustainability”. In: */th IAA/UT Space Traffic Management Conference, Austin, Texas*. 2021.

[13] J. Rodriguez-villamizar and T. Schildknecht. “Daylight laser ranging of space debris with a geodetic laser from the swiss optical ground station and geodyamics observatory zimmerwald : first experiences”. In: May (2021), pp. 20–23.

[14] J Šilha, S Krajčovič, P Zigo, et al. “Development and operational status of AGO70 telescope”. In: *Proceedings of the 8th European Conference on Space Debris, Darmstadt, Germany*. 2021.

[15] J. Silha, S. Krajcovic, D. Zilkova, et al. “Slovak Optical Telescope and Image Processing Pipeline for the”. In: *1st NEO and Debris Detection Conference* January (2019), pp. 22–24.

[16] G. Tommei, A. Milani, and A. Rossi. “Orbit determination of space debris: Admissible regions”. In: *Celestial Mechanics and Dynamical Astronomy* 97.4 (2007), pp. 289–304.